Dissertations and Theses

7-18-2013

Computing Radiation Exchange

Jonathan L. Nutzati Fontaine
Embry-Riddle Aeronautical University - Daytona Beach

Computing Radiation Exchange

Jonathan L. Nutzati Fontaine
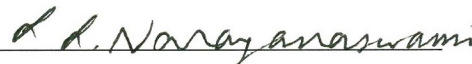
July 18, 2013

Computing Radiation Exchange

By Jonathan L. Nutzati Fontaine

This thesis was prepared under the direction of the candidate's thesis committee chair Dr. Eric R. Perrell, Department of Aerospace Engineering, and has been approved by the members of this committee. It was submitted to the Graduate Studies Office and was accepted in Partial Fullfillment of the Requirements for the Degree of Master of Science in Aerospace Engineering.
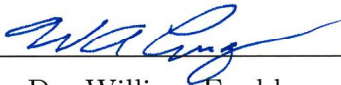
THESIS COMMITTEE

_____
Dr. Eric R. Perrell

_____
Dr. Lakshman Narayanaswami

_____
Dr. William Engblom

_____
Dr. Yi Zhao
Graduate Program Coordinator

_____
Dr. Robert Oxley   7-18-13
Associate Vice President for Academics

ACKNOWLEDGEMENTS

At the completion of my Master's degree, I cannot but look back at my twenty or so years of schooling and wholeheartedly thank my parents for teaching me the importance of education and their continued support and motivation throughout my time here at Embry-Riddle Aeronautical University.

"The universe is probably littered with the one-planet graves of cultures which made the sensible economic decision that theres no good reason to go into space each discovered, studied, and remembered by the ones who made the irrational decision"

- Randall Munroe

ABSTRACT

Author: Jonathan L. Nutzati Fontaine

Title: Computing Radiation Exchange

Institution: Embry Riddle Aeronautical University

Degree: Master of Science in Aerospace Engineering

Year: 2013

A computational tool to simulate thermal radiation between surfaces is developed. The output is verified against cases for which the analytical solutions are available. The tool can be used as a stand-alone program, or as an interactive module for CFD. In such an application the module would augment other heat transfer boundary conditions. The tool is demonstrated by post-processing surface temperature field data from a supersonic CFD calculation. The result is a net thermal radiation surface data field - the black body radiative effluxes as functions of temperature, less the integrated influxes multiplied by their geometric view factors from other surface cells. An algorithm to compute blocking, or "shadowing" of surfaces is presented and demonstrated on a simple geometry. Validations using a geometrically complex experimental case from the literature is performed.

Contents

List of Tables

List of Figures

Nomenclature

Symbol

A	Area
C_P	Specific Heat
E	Emissive Power
E_b	Blackbody Emissive Power
F_{1-2}	View Factor from 1 to surface 2
G	Irradiation
J	Radiosity
q	Heat Flux per Unit Area
R	Resistance
r	Displacement Vector
T	Temperature
ϵ	Emissivity
ϕ	Solid Angle
ρ	Density
σ	Stefan-Boltzmann Constant

I INTRODUCTION

Heat transfer modeling is a significant goal in many CFD solutions, especially in high temperature, supersonic, hypersonic or chemically reacting flows. Radiation accounts for a large percentage of the energy exchange occurring in the nozzles and combustion chambers of jets and rockets. It was felt that there was the potential for a versatile new computational tool to model thermal radiation using finite element analysis.

Radiation is the primary mechanism through which heat is conveyed through deep space and for this reason is also highly relevant to thermal considerations of spacecraft. Spacecraft thermal design must take into consideration performance of electrical components, stability of fluid or fuel storage and, in manned spacecraft, environmental considerations. An accurate thermal radiation simulation software can aid in the design process of spacecraft for a variety of missions without the need to experimentally produce some of the extreme radiation environments experienced in space.

Current radiation modeling capabilities consist largely of Monte Carlo methods. Radiation network modeling as per Oppenheim's method [7] has been previously seen, for example with the Boeing Engineering Thermal Analyzer software. Further developing Oppenheim's method to a finite element approach is the scope of this research.

II THEORY AND EQUATIONS

The fundamental governing equation is the Stefan Boltzmann law. E_b is the Black-body emissive power in Watts per unit area and σ is the Stefan-Boltzmann constant, 5.667×10^{-8} m $\frac{W}{m^2}.K^4$.

$$E_b = \sigma T^4 \tag{II.1}$$

Generally, practical applications use the actual emissive power E , equal to E_b times an emissivity ϵ, a fraction depending on surface material, color, and roughness.

$$E = \epsilon E_b \tag{II.2}$$

The heat transfer between two surfaces i and j, is a function of their areas, emissive powers, and a geometric view factor F_{i-j}, the fraction of radiation leaving surface i that arrives at surface j.

II.1   View Factors
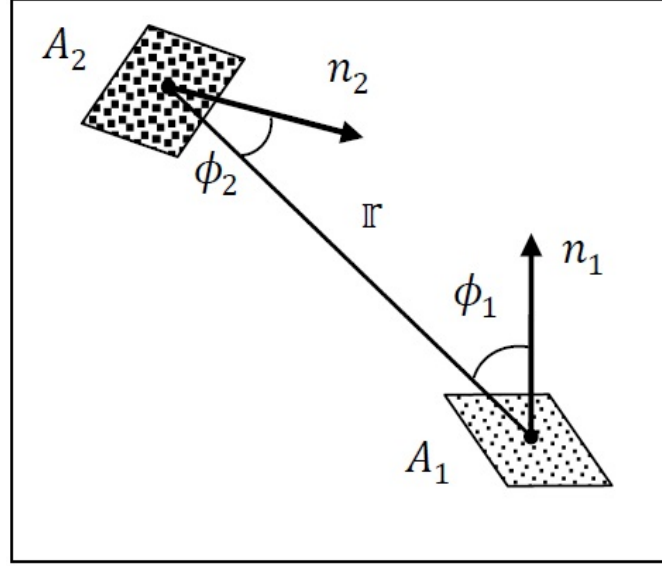
Figure II.1: Visual depiction of view factor formula

Consider differential elements dA_1 and dA_2 of two Blackbody surfaces. If surface 1 were to diffusely emit radiation, some proportion of it, known as the view factor, would strike surface 2. The view factor is dependent on spatial orientation of surface 1 with respect to surface 2 and their relative geometries. It is easily shown that the view factors of dA_1 to dA_2 is:

$$dF_{1-2} = \frac{\cos \phi_1 \cos \phi_2}{\pi r^2} dA_2 \qquad (\text{II.3})$$

And the overall view factor is found by integrating over both surfaces:

$$A_1 F_{1-2} = \int \int \frac{\cos \phi_1 \cos \phi_2}{\pi r_2} dA_1 dA_2 \qquad (\text{II.4})$$

The view factor reciprocity relation is useful in view factor algebra. It states that the view factor from any surface 1 to any surface 2 multiplied by the area of surface one is equal to the return view factor multiplied by the area of surface 2. This can also be inferred from

the symmetry of Equation II.4

$$A_1 F_{1-2} = A_2 F_{2-1} \tag{II.5}$$

II.2 Greybody Assumption

The Blackbody assumption states that all energy that strikes a surface is absorbed. In most real radiative interaction, some percentage of incident radiation is absorbed and the remainder is reflected away from the surface. We define irradiation, denoted by G, as the total radiation incident upon a surface per unit time and per unit area. We define radiosity, denoted by J, as the total radiation that leaves a surface per unit time and per unit area. The net heat flux for a greybody surface will be the difference between its Radiosity and its Irradiation.
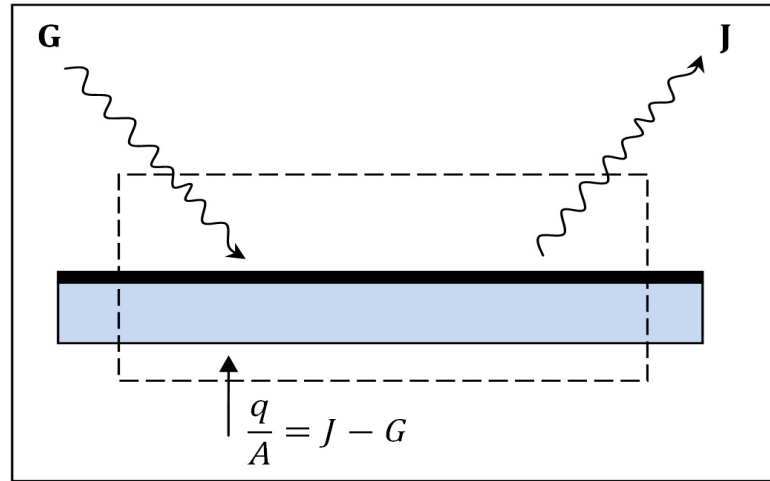
Figure II.2: Illustration of greybody radiation exchange

If we make the assumption that none of the incident radiation is transmitted through the surface, we can define radiosity as the sum of the radiation emitted by the surface and the radiation reflected by the surface as in equation II.6 where ϵ is the emissivity.

$$J = \epsilon E_b + (1 - \epsilon)G \tag{II.6}$$

The greybody assumption as presented in this section assumes that radiation leaving the surface is diffuse, meaning that outgoing radiation exhibits no preferred direction. While this assumption holds well for emitted radiation, it is not always accurate for reflected radiation, which can, depending on surface properties, have a specular quality. Specular reflection refers to when the angle of incidence and the angle of reflection of a ray are equal. Specular radiation is beyond the scope of this research.

II.3   Radiosity Networks

Oppenheim [7] found that it was convenient to model the thermal system by analogy to the electrical circuit as a network of nodes separated by resistors where heat flow is 'current' and emissive powers and radiosities are 'potentials'. Between blackbodies, each surface can be represented by an emissive power node and resistance is simply a function of view factor, a spatial resistance. For greybody surfaces, another node and resistor must be added for each surface to take into account the emissivity, which is effectively a surface resistance. Take for example, Figure II.3, a network representing two greybody surfaces interacting with each other by means of radiation exchange.
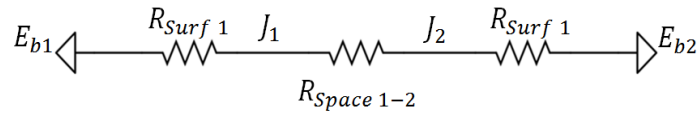
Figure II.3: Radiation network depiction of two surface system

The heat flux per unit area, q, from the Blackbody Emissive Power node on Surface 1 to the Radiosity node of Surface 1 is computed by:

$$q = \frac{E_{b1} - J_1}{(1 - \epsilon_1)/\epsilon_1 A_1} \tag{II.7}$$

By the electrical network analogy, if the heat flux term on the left is current, and the numerator on the right is potential, our denominator is effectively the resistance of the surface.

$$R_{surface} = \frac{1 - \epsilon_1}{\epsilon_1 A_1} \tag{II.8}$$

Of the total radiation leaving surface 1, the amount that reaches surface 2 is:

$$J_1 A_1 F_{1-2}$$

Of the total energy leaving surface 2, the amount that reaches surface 1 is:

$$J_1 A_2 F_{2-1}$$

The net interchange between the two surfaces is then:

$$q_{1-2} = J_1 A_1 F_{1-2} - J_2 A_2 F_{2-1} \tag{II.9}$$

Applying the view factor reciprocity relation, II.5 gives:

$$q_{1-2} = \left(J_1 - J_2 \right) A_1 F_{1-2} \tag{II.10}$$

By the network analogy, if the heat flux term on the left is current, and the radiosities on the right are potential, the reciprocal of the view factor term is effectively the spacial resistance between the surfaces.

$$R_{space} = \frac{1}{A_1 F_{1-2}} \tag{II.11}$$

Then, in order to solve the network, one could apply Kirchhoffs current law as used in DC circuit analysis, stating that the sum of all the currents entering a node is zero. Figure II.4 depicts the simple two surface system of Figure II.3 with the expressions for nodal

resistances displayed.
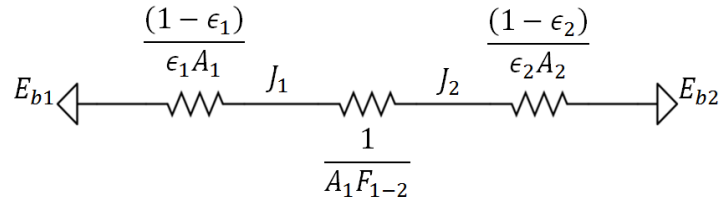
Figure II.4: Radiation network depiction of two surface system

The resistances for "parallel" Radiation circuits are defined likewise by analogy to electrical networks.

II.4   Formulation of Radiosity Networks for Numerical Solution

The numerical solution allows for rapid solving of larger networks with many surfaces. Consider the radiosity node, J_n on surface 'n' in a network with large integer, 'm' visible surfaces as depicted in Figure II.5..
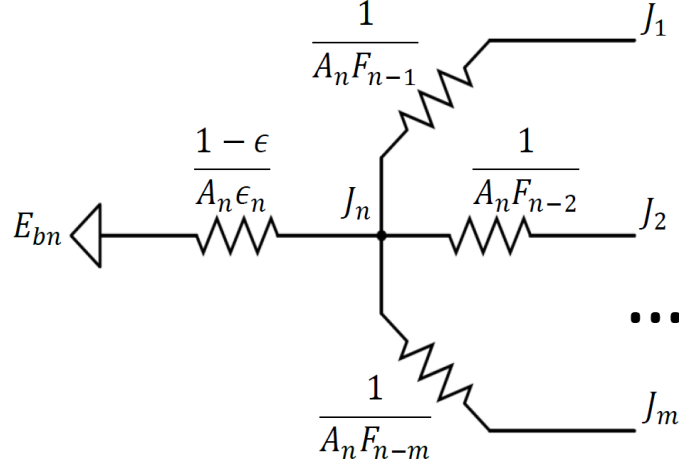
Figure II.5: Network diagram for a general node J_n in a network with many of surfaces

Using Kirchhoff's current law on the J_n node and cancelling the area terms, we obtain the following general equation for heat flux at the radiosity nodes of the network.

$$\frac{\epsilon_i}{1 - \epsilon_i} \left(E_{b_n} - J_n \right) + \sum_m F_{n-m} \left(J_m - J_n \right) = 0 \tag{II.12}$$

This can then be solved in terms of J_n

$$\sum_m J_m A_n F_{n-m} + E_{b_n} \frac{A_n \epsilon_n}{1 - \epsilon_n} = J_n \left(\sum_m A_n F_{n-m} + \frac{A_n \epsilon_n}{1 - \epsilon_n} \right)$$

$$J_n = \frac{\left(\sum_m J_m A_n F_{n-m} + E_{b_n} \frac{A_n \epsilon_n}{1-\epsilon_n} \right)}{\left(\sum_m A_n F_{n-m} + \frac{A_n \epsilon_n}{1-\epsilon_n} \right)} \tag{II.13}$$

In order to obtain the radiosities, we can use a Gauss-Seidel iteration scheme to solve for the coefficients. We use equation II.14 to calculate the radiosities for greybody surfaces of a given temperature and equation II.15 to calculate the radiosities for surfaces with specified heat flux. For insulated surfaces, J_1 is simply E_{b1}.

$$J_n = \left(\frac{\sum_{n \neq m} F_{n-m} J_m + E_{b_n} \frac{\epsilon_n An}{1-\epsilon n}}{\sum_{n \neq m} F_{m-m} + \frac{\epsilon_n An}{1-\epsilon n}} \right) \qquad (\text{II.14})$$

$$J_n = \left(\frac{\sum_{n \neq m} F_{n-m} J_m}{\sum_{n \neq m} F_{m-m}} \right) + \frac{q_n}{A_n} \qquad (\text{II.15})$$

For greybody surfaces, we compute the net heat transfer from the surface by taking the difference of the surface radiosity and the Blackbody emissive power and dividing by the internal resistance of the surface.

$$q_{net_n} = (E_{b-n} - J_n) \frac{\epsilon_n}{1 - \epsilon_n} \qquad (\text{II.16})$$

For surfaces with specified heat flux, the Blackbody emissive power is calculated using II.17 from which we can then obtain the temperature through a simple inversion of the Stefan Boltzmann law as in II.18:

$$E_{b_n} = J_n + \frac{1 - \epsilon_n}{\epsilon_n} \frac{q_n}{A_n} \qquad (\text{II.17})$$

$$T_n = \frac{E_{b_n}^{\frac{1}{4}}}{\sigma} \qquad (\text{II.18})$$

II.4.1 Transient Analysis

If a radiation network is to progress in time, we simply need to increment the temperature for each discrete time step based on the computed Q_{net} for each greybody surface. The temperature differential is dependent upon the properties of the material and is computed from the differential equation:

$$\frac{dT}{dt} = \frac{q_{net_n}}{\rho C_P dx} \qquad (\text{II.19})$$

$$T_n = T_n + dT_n \qquad (\text{II.20})$$

For surfaces with a specified heat flux, the instantaneous temperature is obtained from II.18 at each time step.

II.5   Surface Shadowing (Blocking)

An algorithm was developed that determines whether or not two radiating cells are blocked by another. It is initiated for all non-zero view factors. Once the view factor between any two cells is determined to be non-zero, all other cells on all surfaces in the grid are tested to see if they block. In the algorithm, blocking is defined as the event in which the position vector between the first two cells intersects the third cell. In order to determine if such an intercept occurs we define the plane of the cell and define the radial vector as a line. The co-ordinate of the intercept point between the plane and the line can be obtained using their respective equations and solving for a common parameter, t from which we can then solve for the intercept point.
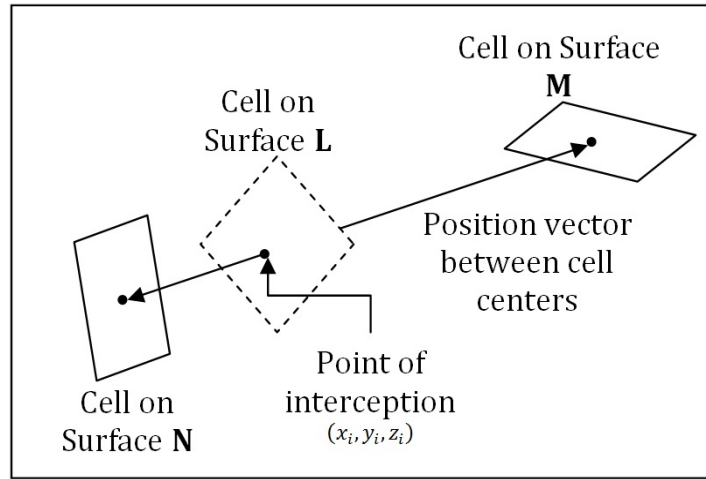
Figure II.6: Testing cells for blocking

Once the coordinates of the intercept point have been computed, it needs to be known whether the intercept point lies within the boundaries of the cell in question. In order to test this, vectors are drawn from all four corners of the cell to the intercept point. As the dot products of the unit vectors, the cosines of the angles between each of these four vectors

10

is obtained and summed up in a clockwise direction. The sum of the cosines between the vectors should make a full circle if the intercept point lies within the cell boundaries. In this case, the view factor is set to zero.
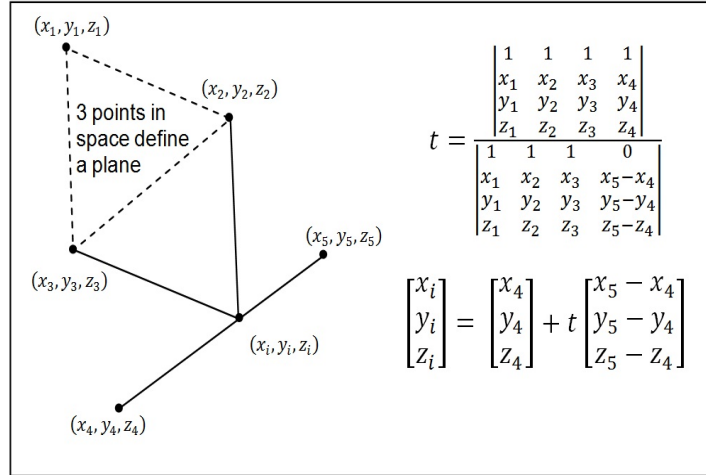
Figure II.7: Finding the interception point

II.6   Background View Factors

Radiation leaving a surface that doesn't strike any other surfaces must be taken in by the background. If the total view factor from any surface is unity, we can find the fraction of radiation emitted to the background by subtracting the sum of all view factors from 1. We can infer that any fully enclosed cell with have a view factor to the background of zero.

$$F_{n-background} = 1 - \sum_{n \neq m} F_{n-m} \tag{II.21}$$

III COMPUTATIONAL APPROACH TO THE PROBLEM

The basic approach is to compute the view factors, hence radiation heat transfer rates between each pair of surface cells in a computational grid.

1. Compute and store view factors for differential surface elements (grid cells) the integrand in our double surface integral, Equation II.4.

2. For each pair of surface elements, query all other surface elements to determine blocking, or shadowing. If a surface element pair is blocked by another surface element, assign a view factor of zero for the pair.

3. Compute also the view factors to the environment (background) for each surface element. Normally this is unity minus the sum of all other view factors. For surfaces radiating from both sides, this will be two minus the sum.

4. Form given surface temperature field and emissivities, and construct radiosity network equations.

5. Solve radiosity field using Gauss-Seidel relaxation and Equations II.15 and II.14. On first time step, initialise with $J = \epsilon E_b$. On subsequent time steps, initialise with previous solution for Js.

6. Compute net heat flux from each cell using Equation II.16 for Greybodies.

7. Advance solution in time with lumped heat capacity approximation for each surface element using assigned or assumed values for material thickness, density, specific heat, and time step. Use Equation II.19 to get Temperature changes for the timestep.

8. For surfaces with specified heat flux, calculate temperatures from emissive power with Equations II.17 and II.18

9. Go to 4. and iterate to convergence.

IV   CALCULATIONS

The software was designed to operate with structured surface grids in three dimensions. Grid refinement studies are conducted for several of the calculations performed in the following sections.

IV.1   Verification of View factors

View factors have been calculated by performing the integral in Equation II.4 for some simple geometric surface arrangements, shown in Figure IV.1, that have known analytical solutions.
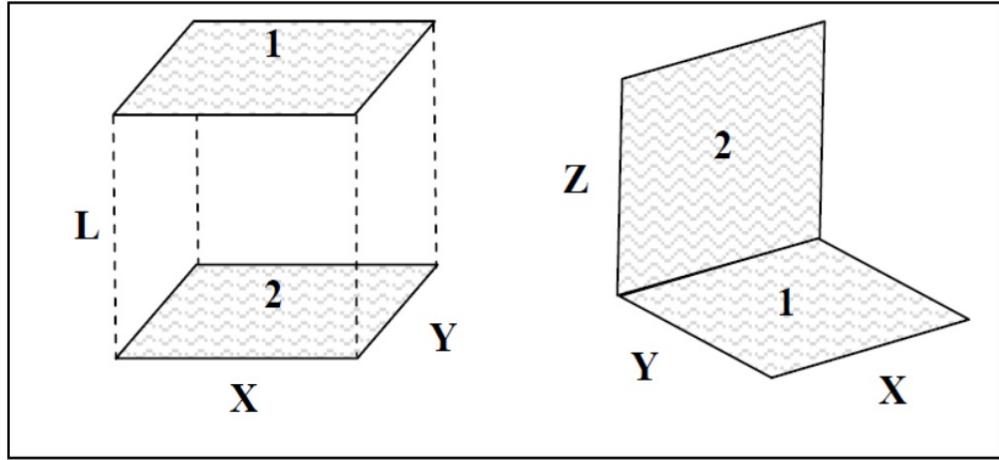
Figure IV.1: Model cases for analytical view factors

Closed form solutions taken are from Holman [1] for the parallel, equal rectangles and perpendicular rectangles with one shared edge.

14
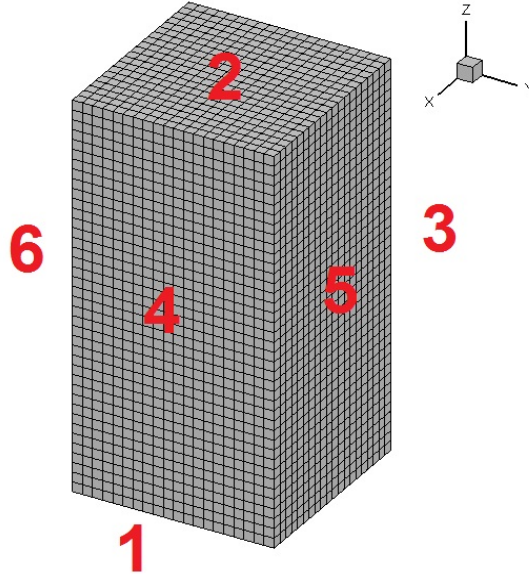
Figure IV.2: Grid used in verification and grid refinement study for view factors

A rectangular prism shaped grid was built to reproduce the view factor model cases for the code. Figure IV.2 shows the grid with dimension 20 x 20 x 40. Results are presented in Table IV.1.

Table IV.1: View factors from grid refinement study

Participating Surface		Integrated View Factor			
From	To	5 x 5 x 10	10 x 20 x 20	20 x 40 x 40	Analytical
1	2	0.0689376	0.06876136	0.068611242	0.06861
1	6	0.2595203	0.2462894	0.2395966	0.23960
5	6	0.2669109	0.2539746	0.2473534	0.24736
4	6	0.2883339	0.2864841	0.2860243	0.28603

IV.2   Concept Demonstration

The case used was an inviscid supersonic flow through a rectangular duct with an asymmetrical swept ramp, computed with Hyp [2,3], an MPI parallel multi-block CFD code using Steger-Warming [4] flux vector splitting. A shock is produced in the ramp and is reflected down the duct which provides the surface temperature distribution on the boundaries.
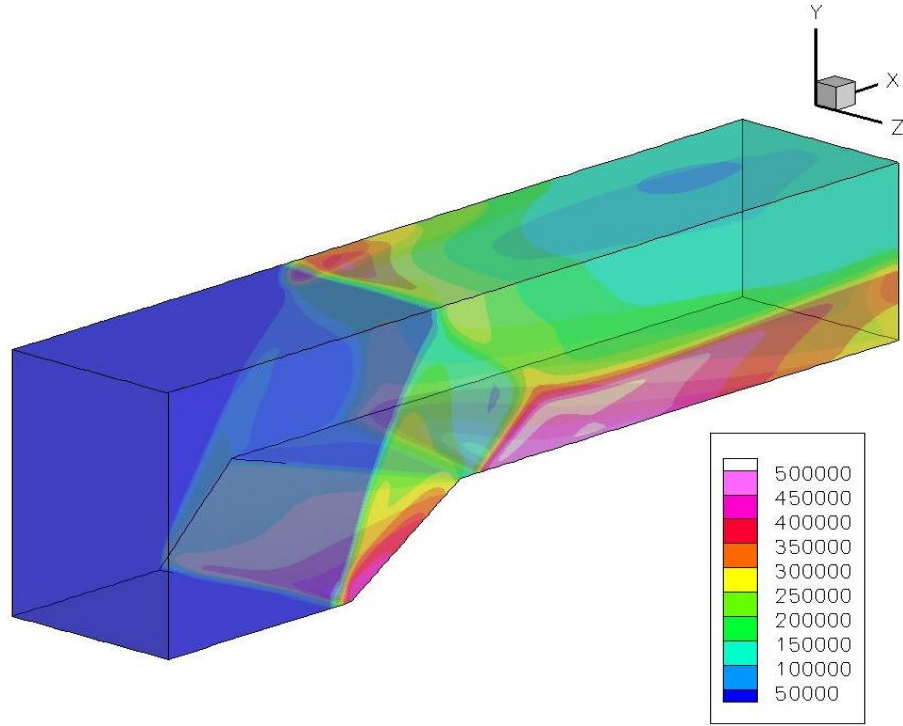
Figure IV.3: Blackbody emissive power field

Figure IV.3 shows the Blackbody emissive power across the ramp in W/m^2. This value is a function of the temperature field produced at the boundary as a result of the flow. Three locations in the contours where the shock impinges on the duct can be clearly seen from the figure.
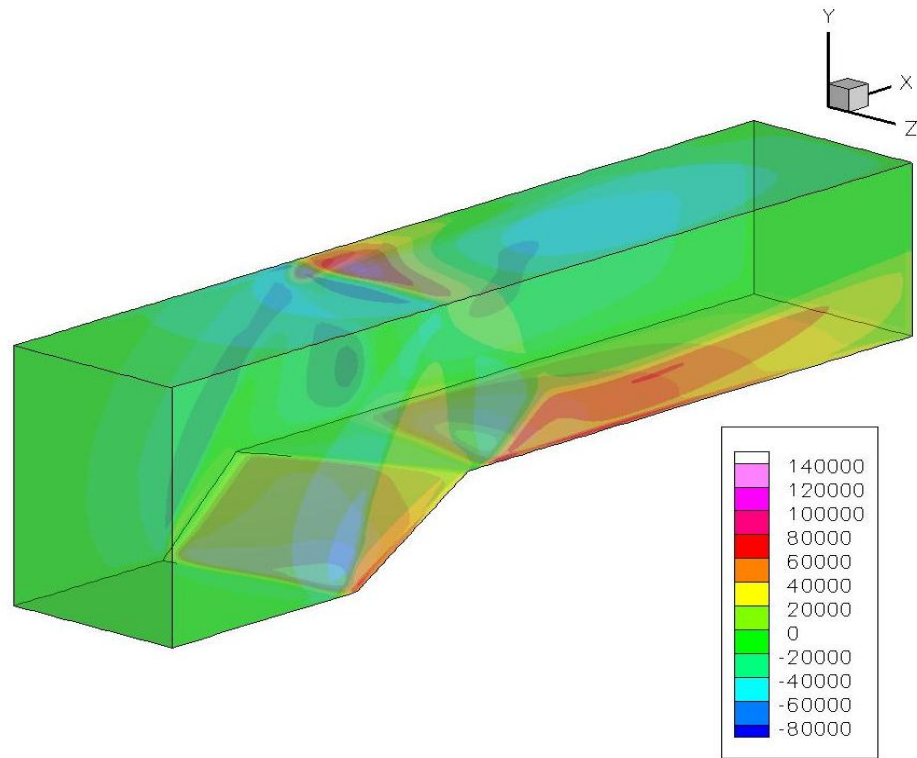
Figure IV.4: Net heat transfer field

Figure IV.4 shows the actual heat exchange in Watts per square meter calculated by the code. Negative values, signify a net inflow of heat while positive values signify a net outflow of heat.

IV.3 Verification of Radiation Module
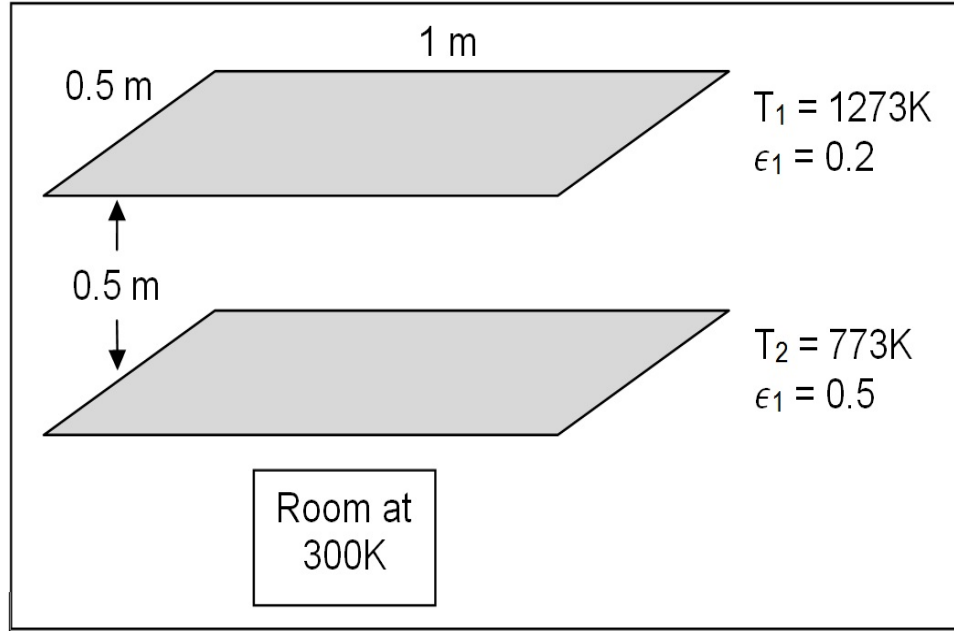
Figure IV.5: Example 8-6

Example problem 8-6 from [1] involves calculating the heat exchanged between two equal parallel plates spaced at half a meter apart and the surrounding room. To replicate the solution, a grid was produced with two surfaces at 100 x 50 cells each.

The view factors are computed between the surfaces as in the parallel square plates model case. The view factors from each plate to the room, denoted as surface 3, are then calculated using the view factor reciprocity theorem.

$$F_{1-2} = F_{2-1} = 0.285$$

$$F_{1-3} = (1 - F_{1-2}) = 0.715$$

$$F_{2-3} = (1 - F_{2-1}) = 0.715$$

Blackbody emissivities are computed for both surfaces and the surrounding room

using the Stefan Boltzmann law and their respective temperatures. View factors from each plate to the room, denoted as surface 3, are then calculated using the view factor reciprocity theorem.

$$E_{b1} = 148.87 kW/m^2$$

$$E_{b2} = 20.241 kW/m^2$$

$$E_{b3} = 0.4592 kW/m^2$$

Resistances in the network are then calculated using emissivities for the resistances between surface nodes and radiosity nodes and view factors for the resistances between radiosity nodes as described in II.3.

$$\frac{1 - \epsilon_1}{\epsilon_1 A_1} = \frac{1 - 0.2}{(0.2)(0.5)} = 8.0$$

$$\frac{1 - \epsilon_2}{\epsilon_2 A_2} = \frac{1 - 0.5}{(0.5)(0.5)} = 2.0$$

$$\frac{1}{A_1 F_{1-2}} = \frac{1}{(0.5)(0.285)} = 7.018$$

$$\frac{1}{A_1 F_{1-3}} = \frac{1}{(0.5)(0.715)} = 2.797$$

$$\frac{1}{A_2 F_{2-3}} = \frac{1}{(0.5)(0.715)} = 2.797$$

The radiosities are obtained by solving the heat transfer network for the problem. Setting the sum of the radiosities to zero and solving the set of simultaneous equations.

$$\frac{E_{b1} - J_1}{8.0} + \frac{J_2 - J_1}{7.018} + \frac{E_{b3} - J_1}{2.797} = 0$$

$$\frac{J_1 - J_2}{7.018} + \frac{E_{b3} - J_2}{2.797} + \frac{E_{b2} - J_2}{2.0} = 0$$

Plugging in the values for the Blackbody emissivities into the equations above gives

the following radiosities.

$$J_1 = 33.469 kW/m^2$$

$$J_2 = 15.05 kW/m^2$$

With the radiosities it is now possible to plug in and solve for the net heat transfer from each surface to the other surface and from each surface to the room.

$$
\begin{aligned}
q_1 &= \frac{E_{b1} - J_1}{(1 - \epsilon_1)/\epsilon_1 A_1} \\
&= \frac{148.87 - 33.469}{8.0} \\
&= 14.425 kW
\end{aligned}
$$

$$
\begin{aligned}
q_2 &= \frac{E_{b2} - J_2}{(1 - \epsilon_2)/\epsilon_2 A_2} \\
&= \frac{20.247 - 15.054}{2.0} \\
&= 2.594 kW
\end{aligned}
$$

$$
\begin{aligned}
q_1 &= \frac{J_1 - J_3}{1/A_1 F_{2-3}} + \frac{J_2 - J_3}{1/A_2 F_{2-3}} \\
&= \frac{33.469 - 0.4952}{2.979} + \frac{15.054 - 0.4592}{2.979} \\
&= 17.020 kW
\end{aligned}
$$

The code was made to run through example problem 8-6 again but using grids of differing coarseness. Results are shown in the following table.

Table IV.2: Heat transfer rates and grid refinement study for Example 8-6

	5 x 10	10 x 20	20 x 40	50 x 100	Analytical
Heat lost by surface 1 (kW)	14.42521	14.42877	14.42965	14.42993	14.425
Error	0.00146%	0.002614%	0.03224%	0.03418%	0.00000%
Heat lost by surface 2 (kW)	2.556651	2.573773	2.577998	2.579176	2.594
Error	1.43982%	0.77976%	0.61689%	0.57147%	0.00000%
Heat absorbed by the room (kW)	16.981851	17.002472	17.007569	17.009254	17.020
Error	0.22414%	0.10298%	0.07304%	0.06314%	0.00000%

IV.4   Verification of the Blocking Algorithm

The blocking algorithm concept and implementation are demonstrated graphically in Figure IV . The contours are view factors from the position indicated, with zero view factors (blue region) assigned for cells which meet the blocking criterion above.
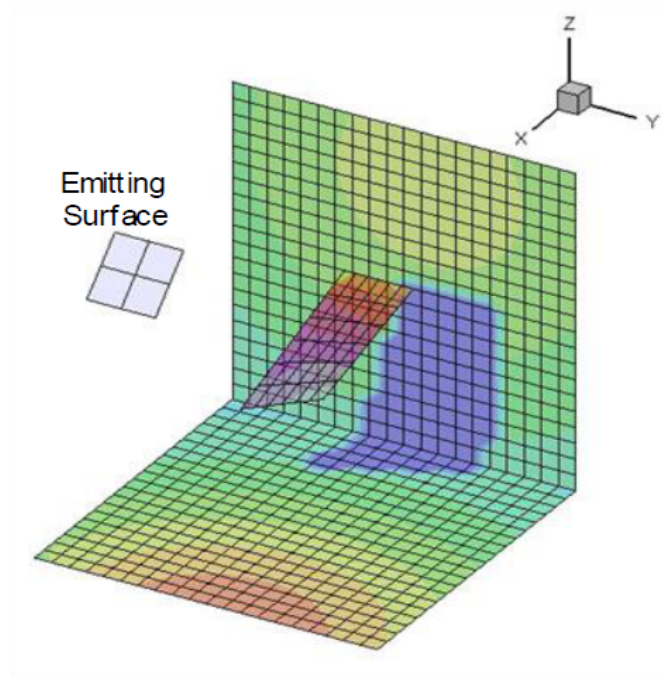
Figure IV.6: Oblique shadows rendered on a corner

The source of the incoming radiation in Figure IV.6 is the small, white elevated surface above the oblique surface and backdrop. The blue contours represent the regions of the grid where there is no visibility to the radiation source. Similarly in Figure IV.7, the regions in the darkest blue are shadowed from the source, located near the top of the heater on the right.
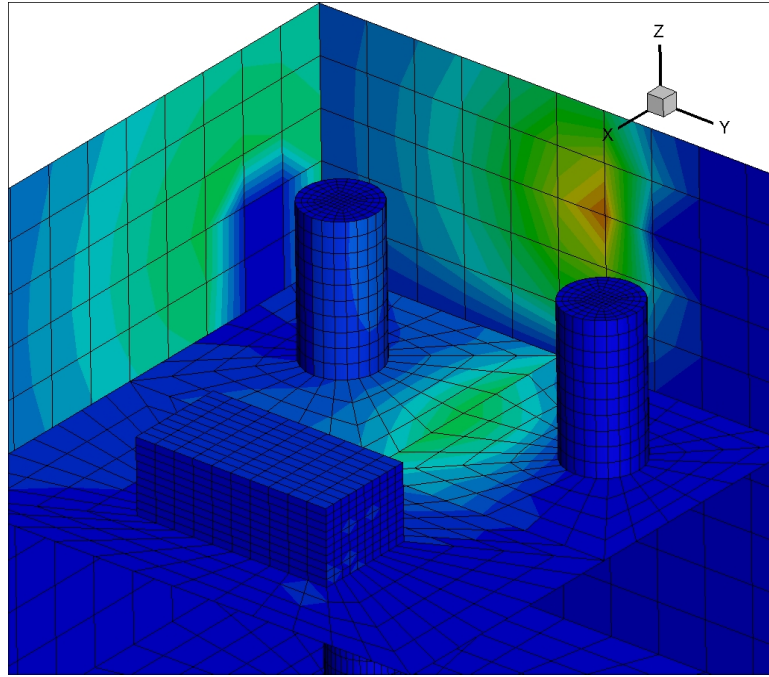
Figure IV.7: Example of blocking with complex geometry

V VALIDATION
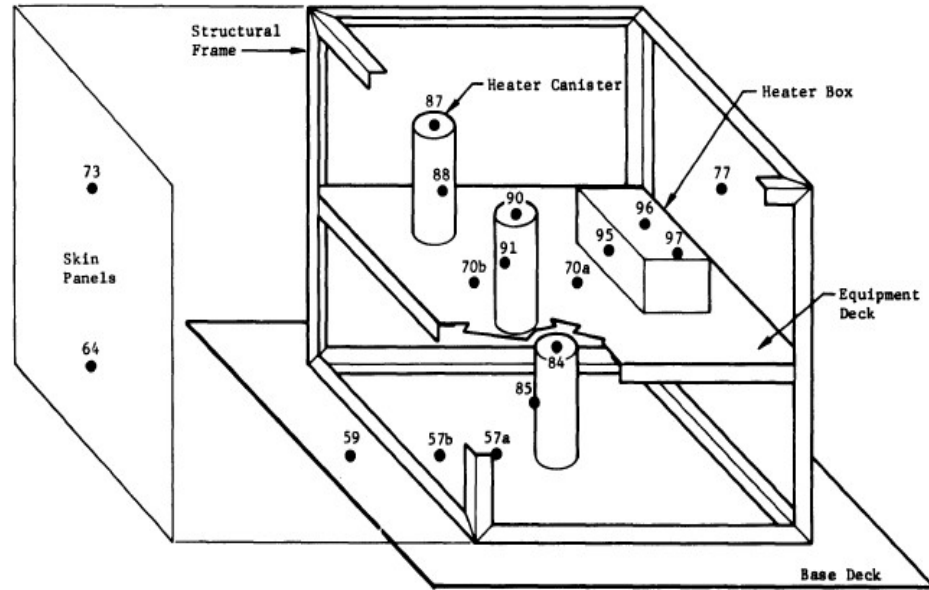
Figure V.1: Simulated spacecraft prototype from Boeing experiment

V.1 Experimental set-up

In 1969, the Boeing Company performed a series of both experimental and numerical thermal tests on a mock prototype spacecraft in order to verify an in-house thermal design software called the Boeing Engineering Thermal Analyzer (BETA) and to investigate the scalability of thermal modeling. While the prototype chosen does not resemble any spacecraft in appearance it simulates the physics of interest through the following characteristics:

1. Lightweight exterior skin panels

2. A relatively heavy structural frame

3. An overextended base deck resulting in solar reflections back onto exterior surfaces

4. Energy sources interior to the spacecraft in discrete compartments to simulate electronic components

A wealth of thermal data was collected from thermocouples placed through the prototype as well as the relevant testing conditions presented in [5] and [6]. This study was chosen as an excellent experimental benchmark with which to validate the software.

Table V.1: Radiative properties of prototype features

Material	6061-T6	7075-T6
Emissivity	0.843	0.875
$\rho C_P (J/m^3 - K)$	2,441,731	2,422,954
Features	Equipment Deck Base Deck Closure Deck Skin Panels Heater Shell (Canister)	Heater Shell (Box)

The prototype was set up in the Boeing space environment simulator with the chamber being supercooled to 100K by liquid Nitrogen and capable of absorbing up to $1076 W/m^2$ while maintaining that temperature. The temperature field is then developed through the action of heat sources in the form of four electric heaters inside of the prototype and the solar simulator positioned above it.

The experimental set-up of the Boeing configuration, as with any real thermal system radiates heat to the surroundings, in this case a supercooled shroud of emissivity 0.9. A verification of the performance of the background view factor would yield zero values for cells totally surrounded by other surfaces, such as the interior spacecraft components.

All internal surfaces in the Boeing prototype are coated with a flat black thermal coating of emissivity 0.841 except for the side surface of heater 4 facing across the equipment deck towards heaters 2 and 3 which was polished aluminium with emissivity 0.055. Similarly,

outer surfaces were coated with a B-1060 white thermal coating of emissivity 0.894 except for the outer surface of the closure deck which was also polished aluminium.

V.2 General Assumptions and Simplifications

The prototype is reinforced by structural frame made of 1" x 1" 6061-T6 aluminium angle with a web of 0.125inch, to which the walls, base deck and closure deck are bolted. This material used is the same as the majority of the prototype and the exposed area of the structural members comprises a very small percentage of the total area of the surfaces they are in contact with. The structural frame will be neglected from the thermal analysis.

In the prototype, the canisters and the box are loaded with electrical heating components as shown in Figure V.1. The detailed radiation field internal to the heater box and canisters is not computed. Rather, the heat source is assumed to be projected evenly onto the inner surface of the heater canister. This assumption is supported by the conclusions of MacGregor [5] who found their numerical results to be comparable.

With the exception of the heater surfaces, all surfaces in the grid radiate from both sides. Activated heaters are set to neglect internal radiation from the analysis. As per the network method in Holman [1], heaters are modeled by a quasi steady-state approximation inherent to Equations II.17 and II.15.

V.3 Boeing Engineering Thermal Analyzer

The BETA program is a simple network solver using relaxation techniques to solve for equilibrium temperatures, and forward differencing to compute transient temperatures. The numerical model involves dividing the prototype and the space simulator chamber into a finite number of isothermal nodes connected by both radiation and conduction paths. Convection is neglected from the analysis.

The interchange factors between the nodes were computed by a separate program

called The Boeing Radiative Interchange Factor program. This program uses a Monte Carlo method to simulate a single photon as it is emited from a surface according to a specified distribution and follows it as it travels through the system, reflecting off surfaces until it is eventually absorbed. This is done for large numbers of iterations to provide an equivalent to radiation nodal resistances that can be input to the network supplied to BETA for solving.

V.4 Replication of Boeing Test Sequences

The test sequences replicated along with their source information is provided in Table V.2. Once the simulation is run to steady state, temperature samples were taken at the points in the grid in closest proximity with the thermocouples, placed at those nodes displayed in Figure V.1. The results are then compared with the thermocouple readings and the corresponding results obtained from BETA.

Table V.2: Replicated test sequences

Test	Heat Sources Active	Power (Watts)
3	Heater 1	35.169
	Heater 2	17.684
5	Heater 3	23.445
	Heater 4	35.168

V.4.1 Test 3
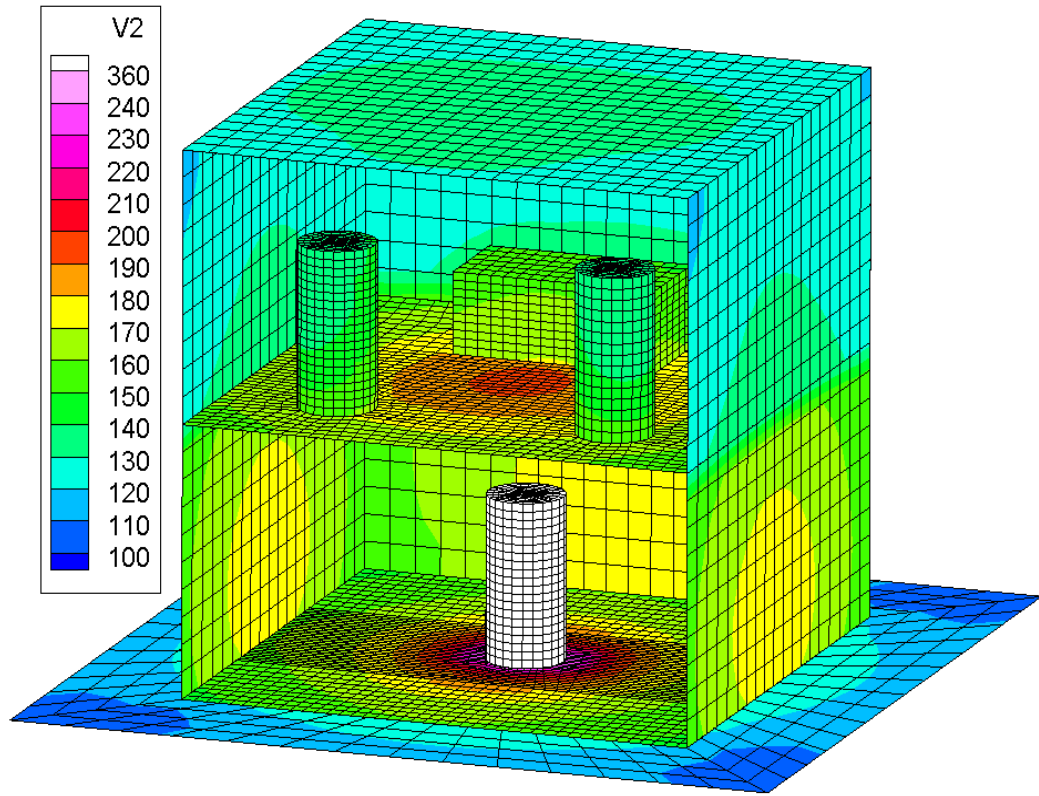
Figure V.2: Steady state temperature field for test 3

In test 3, only heater 1 on the base deck is active while the remaining heaters are off and function as ordinary surfaces in the network. Radial contours can be seen in V.2 emanating from the maxima of the integrated view factors. These hot zones appear directly around the base of the cylinder, on each of the four walls of the prototype and on the equipment deck immediately over the top surface of the cylinder. Decreasing temperature gradients extend from the center of each maximum to the surface edges. The high temperature region on the equipment deck appears to re-radiate to form a secondary warm zone on the closure deck and temperature gradients on the equipment deck heater surfaces.

Table V.3: Steady state results for test 3

Feature	Node	Experimental Results (K)	Numerical Results (K)	Error	BETA Numerical Results (K)	Error
Base Deck	57a	178.44	183.78	2.99%	164.78	8.29%
	57b	158.67	163.33	2.94%	164.78	3.71%
	59	153.83	124.56	19.03%	139.06	10.63%
Heater 1	84	223.83	362.67	62.03%	209.00	7.10%
	85	218.00	361.38	65.77%	203.11	7.33%
Equipment Deck	70a	148.11	195.99	32.32%	141.67	4.55%
	70b	149.06	362.67	143.31%	141.67	5.22%
Heater 2	87	148.11	138.58	6.43%	140.83	5.17%
	88	148.11	151.19	2.08%	140.83	5.17%
Heater 3	90	148.61	138.81	6.59%	140.78	5.56%
	91	148.11	135.62	8.44%	140.78	5.21%
Heater 4	95	148.61	164.48	10.68%	141.00	5.40%
	96	148.11	156.18	5.45%	140.89	5.13%
	97	148.11	152.10	2.70%	140.83	7.22%
External Skin	64	151.00	174.26	15.40%	141.72	6.55%
	73	146.67	131.16	10.57%	139.00	5.52%

Comparing the steady state temperatures with those from the experiment and from BETA, it can be seen that there is fair agreement across the majority of the measured nodes. Numerical results trend higher for most of the nodes with the exception being those nodes in direct contact with the heater surfaces where the temperatures are greatly overestimated. The temperatures for the equipment deck nodes within the view factor maximum from Heater 1 are also significantly overestimated.
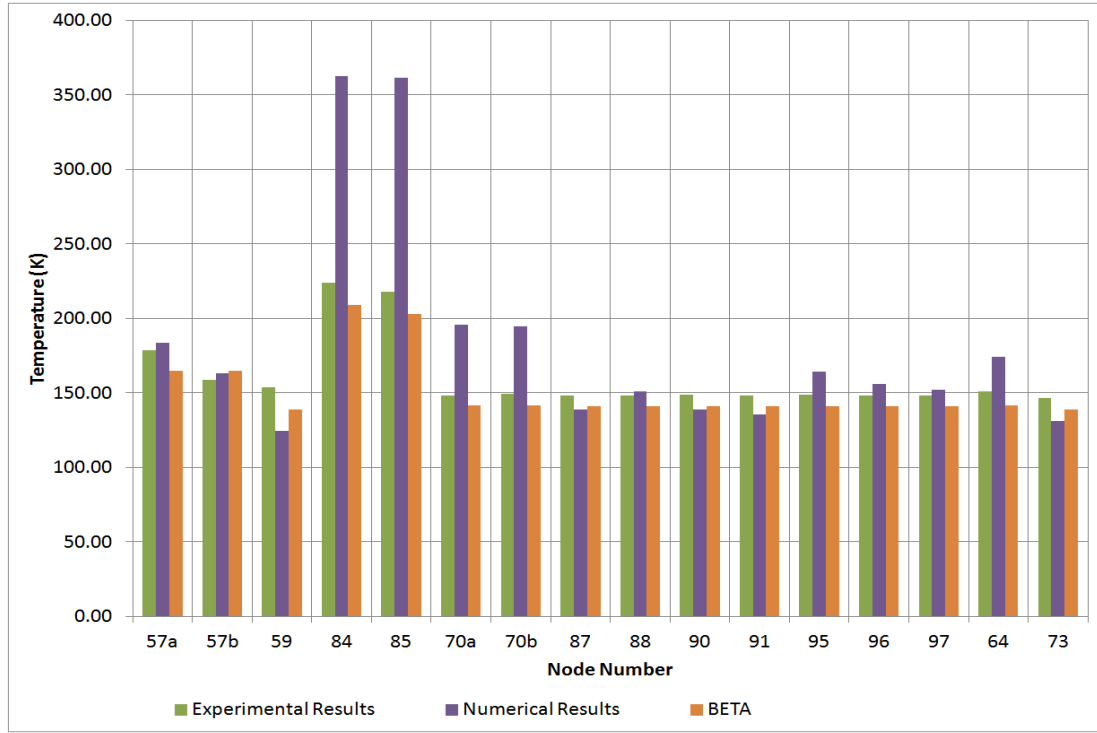
Figure V.3: Steady state temperatures for test 3

A grid refinement study was conducted for Test 3 to determine the effects of refining or coarsening the grid on the accuracy of the results. The temperatures obtained are presented in Table V.4. It was found that although there was very close agreement between the two sets of results as can be seen from Figure V.4, the plots produced from the course grid results were unable to fully resolve the temperature contours. As a results, final results for both tests were obtained using only the fine grid.

Table V.4: Grid refinement study Temperatures (K) for test 3

Feature	Node	Numerical - Coarse Grid
Base Deck	57a	183.78
	57b	163.33
	59	124.56
Heater 1	84	362.67
	85	361.38
Equipment Deck	70a	195.99
	70b	194.61
Heater 2	87	138.58
	88	151.19
Heater 3	90	138.81
	91	135.62
Heater 4	95	164.48
	96	156.18
	97	152.10
External Skin	64	174.26
	73	131.16
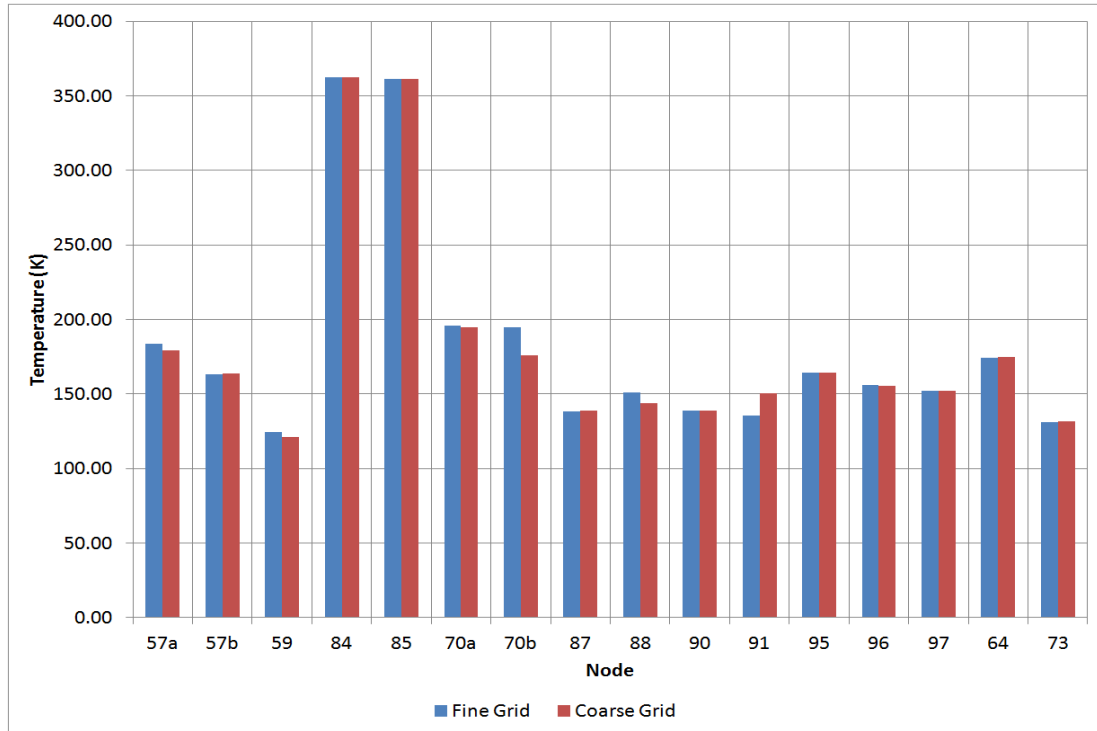
Figure V.4: Steady state temperatures for test 3 grid refinement

V.4.2   Test 5
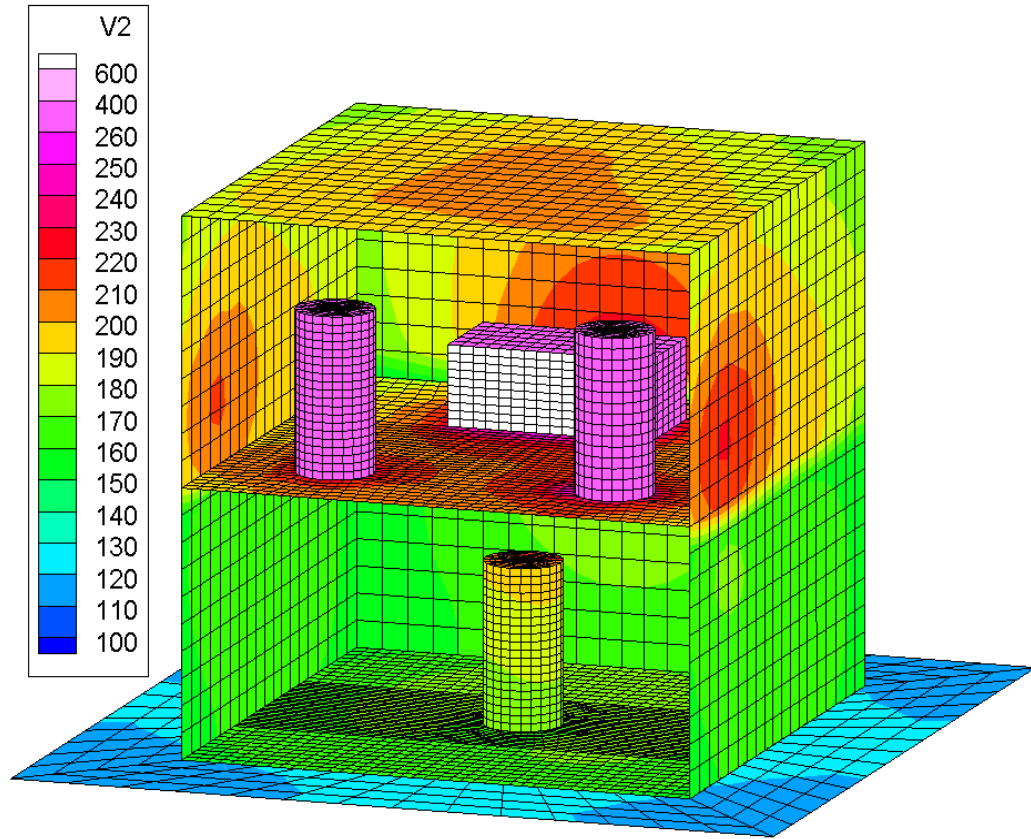
Figure V.5: Steady state temperature field for test 5

In test 5, all of the heaters on the equipment deck are activated with output as per Table V.2. The base deck and bottom half of heater one are for the most part significantly colder than the equipment deck and its features. The asymmetry of the temperature contours seen on the closure deck and opposing sides of the external skin are a result from the uneven power output supplied by the heaters, see Table V.2.

Table V.5: Steady state Temperatures for test 5

Feature	Node	Experimental	Numerical	Error	BETA	Error
Base	57a	172.2	168.4	2.24%	168.4	2.21%
Deck	57b	172.2	166.2	3.50%	168.4	2.21%
	59	170.9	123.5	27.71%	167.2	2.17%
Heater 1	84	173.6	208.7	20.21%	169.3	2.48%
	85	172.7	182.7	5.81%	169.2	2.03%
Equipment	70a	200.7	216.1	7.70%	199.7	0.50%
Deck	70b	199.0	210.5	5.76%	199.7	0.35%
Heater 2	87	214.4	314.2	46.51%	206.2	3.82%
	88	212.9	323.9	52.13%	202.4	4.93%
Heater 3	90	219.2	334.5	52.60%	211.9	3.33%
	91	216.0	337.1	56.06%	207.4	3.98%
Heater 4	95	212.5	610.6	187.32%	215.8	1.55%
	96	218.8	316.7	44.76%	223.4	2.10%
	97	210.1	316.5	50.62%	214.4	2.05%
External	64	180.1	165.0	13.28%	177.2	1.61%
Skin	73	184.7	204.0	10.69%	181.9	1.52%

Across all the nodes, all of the recorded temperatures overestimate the experimental results to some degree except for those at two nodes, node 64 on the lower half of the external skin and node 59 on the exposed section of the base deck outside of the external skin.

Node 59, upon inspection shares no primary visibility with any of the heater surfaces but shares visbility with the temperature maxima on the external skin adjacent to heaters 2 and 3. The view factors between the surfaces are minimal due to the steep incidence angle.

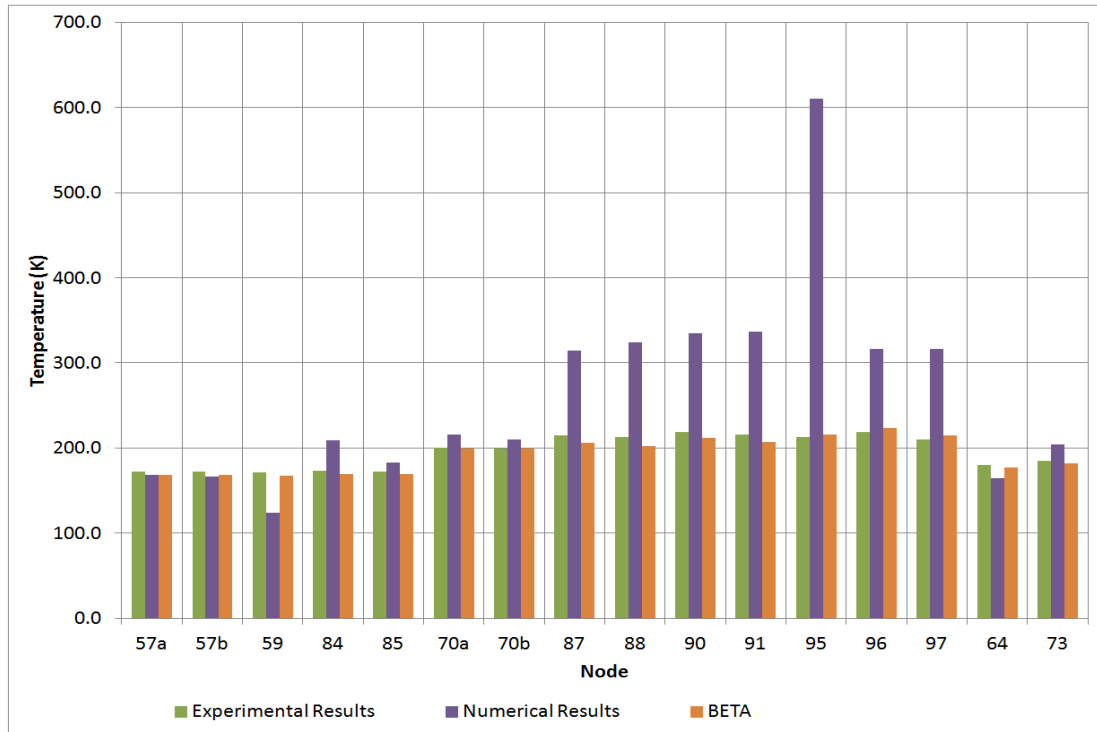**Figure V.6: Steady state temperatures for test 5**

V.5   Discussion of Validation

The trend for tests 3 and 5 was for the temperature of active heaters to be greatly overestimated. Nodes visible to the heater surfaces were overestimated to varying degrees while nodes in close proximity to the temperature maxima were also overestimated. Steep thermal gradients appeared on the deck and skin surfaces.
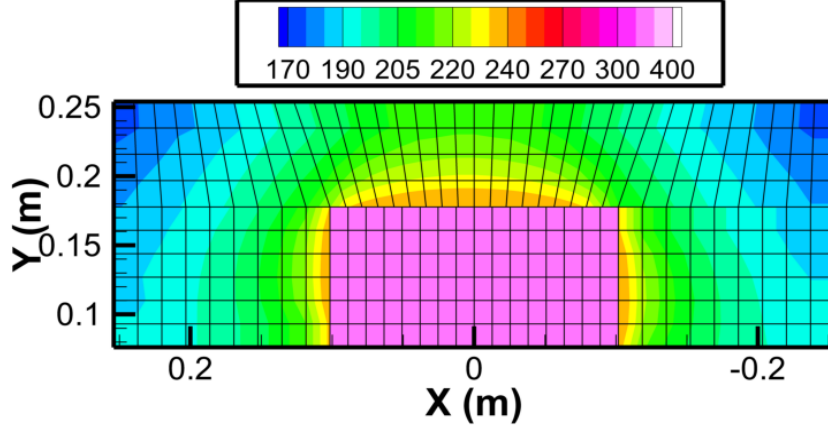
Figure V.7: Steep thermal gradients surrounding Heater 4 in Test 5

The steady state reached with the current numerical method is in radiative equilibrium, however, conduction has not been taken into account. Using the temperature field from test 5, a rough conduction analysis can be performed on some of the cells surrounding the heater where thermal gradients are still significant. It should be noted that adjacent cells on a flat surface cannot directly interact through radiation as the view factor between them is zero.

A one-dimensional snapshot, consisting of a single row of cells is taken of the zone of the equipment deck connecting one side of heater 4 with the external skin. Using the thermal conductivity of Aluminium 6061-T6 as $167.19 \frac{W}{m.K}$, the thickness of the equipment deck and the size of each cell in the one-dimensional snapshot, conduction heat transfer can be approximated across the gradient with Equation V.1.

$$q = \frac{-kA}{\Delta.x} (T_2 - T_1) \qquad \text{(V.1)}$$

Table V.6: Cell by cell one dimensional heat flux by conduction on equipment deck

Cells from Heater	0	1	2	3	4	5	6	7	8	9
Δ X	0	0.0169	0.0339	0.0508	0.0677	0.0847	0.1016	0.1185	0.1355	0.1524
T(K)	230.8	214.8	207.7	202.6	198.9	196.1	193.9	191.9	190.6	190.6
q(W)	-	8.460	3.754	2.697	1.956	1.1480	1.163	1.057	0.687	0

The heat fluxes in this analysis immediately suggests that the effects of conduction are significant across the equipment deck and likely affect the steady state results. A rough integration of the heat fluxes in the equipment deck immediately surrounding heater 4 yields a total conduction heat flux of almost 300W at radiative equilibrium. This unresolved flux can likely account for the significant temperature overestimations at the heater surface nodes for all tests.

In Ref[5] it was stated that the equipment deck was designed at double the thickness of the other surfaces to provide a conduction path from the heater components on the equipment deck to the external skin. One of the assumptions made in Section V.2 was to neglect the aluminium angle supports of the prototype structure. These also provide a conduction path at the edges of each of the decks and skins that should work to equalize surface temperature gradients.

VI CONCLUSIONS AND LIMITATIONS

A Fortran 90/95 computational module that computes radiation view factors for elements of surface meshes has been developed. The integrated view factors for two surface meshes are computed numerically and compared with analytical solutions. In each of three test cases the numerical results were within three percent of the analytical, with an average error of 1.44%.

The tool is exercised on a surface temperature field from a supersonic CFD calculation, to produce a radiation heat flux field. The fluxes are the net of black body efflux differences integrated with their view factors over all surfaces. The tool is used as a simple post-processor in this demonstration, but its interactive use with CFD for augmenting thermal boundary conditions in unsteady calculations should be straightforward.

An algorithm is developed for use with complex geometries in which some surfaces block others. In such cases, view factors in the shadow are set to zero. The algorithm is implemented in the computational tool. Contour plots of view factors from a single point, in which a reasonable shadow is evident, are generated for a various cases to verify the blocking algorithm.

The complete radiant heat transfer finite element analysis package has been validated against experimental results and has yielded a nominally plausible result.

Without any major modifications, the software package could be used to model the exchange of visible light. The need for this application has been established in physics community and the computer graphics industry.

VII RECOMMENDATIONS FOR FUTURE WORK

At present, the tool can model radiation interaction with fluid flow only via boundary conditions. In some high temperature flows, e.g. reentry and rocket combustion, substantial thermal radiation originates within the fluid, away from bounding surfaces. Similarly, the fluid can be absorptive and reflective. Incorporating participating media is a larger challenge, both theoretically and computationally but necessary in order to effectively couple the tool with CFD solutions and combustion modeling. Viskanta and Mengüç [13] provide a comprehensive treatment of current methods to model radiation in participating media. Hassanzadeh gives a more modern treatment i.e. the widely used P_N method with CFD solvers and the Q_L method.

The tools most promising application at this point is toward the thermal modeling of spacecraft or celestial bodies in their interactions with spacecraft and each other. As a stand-alone program it would be important in subsequent versions of the code to add a conduction modeling capability to account for a potentially sizable portion of the heat transfer within a spacecraft among its own surfaces. Perrell, et al, for example, have developed such a model [10], as have Fletcher [8], and Engblom at. al [9]. Apart from the radiation of celestial bodies, it would be rare to find applications or scenarios that can be accurately modelled through pure radiation without any conduction.

Still more accuracy and functionality could be obtained by better refining the radiation model to account for specular radiation, transmissive surfaces and temperature-dependent radiative properties, which can be accounted for with some revisions to the radiation net-

working model.

REFERENCES

1. Holman, J.P., Heat Transfer, 10th ed., McGraw-Hill, New York NY, 2010, Chaps. 8.

2. Hyp, High Speed Thermophysics and Fluid Dynamics Program, Eric Perrell, FL 2003.

3. Perrell, E.R., Erickson, W.D., Candler, G.V., "Numerical Simulation of Nonequilibrium Condensation in a Hypersonic Wind Tunnel, J. Thermophysics and Heat Transfer, (10) 2, 277-283, Apr-June 1996.

4. Steger, J.L., Warming, J.F., "Flux Vector Splitting of the Inviscid Gasdynamic Equations with application to Finite Difference Methods, J. Computational Physics, (40) 2, 263-293, Apr 1981.

5. MacGregor, R.K., "Limitations in Thermal Similitude, The Boeing Company, NAS 8-2 14 22, Aerospace Systems Division Seattle, Washington, 1969

6. MacGregor, R.K., "Spacecraft Design Verification Through Modeling, The Boeing Company, AIAA Paper No. 71-439, Seattle WA, 1969

7. Oppenheim, A.K, "Radiation Analysis by the Network Method", American Society of Mechanical Engineers, Berkeley CA, 1956

8. Fletcher, B.R. "Validation of Conjugate Heat-Transfer Capability for Water-Cooled High-Speed Flows", Embry-Riddle Aeronautical University, Daytona Beach FL, 2007

9. Engblom, W.A., Fletcher, B.R., Georgiadis N.J., "Validation of Conjugate Heat-Transfer Capability of Water-Cooled High-Speed Flow", AIAA Thermophysics Conference, Miami FL, 2007

10. Perrell, E.R., Power, G.D., Robinson, R. "A Modular Conjugate Heat Transfer Capability for the Wind-US CFD Code", AIAA Aerospace Sciences Meeting, Orlando FL, 2010

11. Hassanzadeh, P "An Efficient Computational Method for Thermal Radiation in Participating Media", University of Waterloo, Waterloo ON Canada, 2007

12. Viskanta, R. and Mengüc, M. P. "Radiation Heat Transfer in Combustion Systems", Purdue University, Lafayette IN, 1987

13. Walton, G.N. "Calculation of Obstructed View Factors by Adaptive Integration", NISTIR 6925, Greenberg MD, 2002

14. Xing, C.Y, Sun, S.Z., Grimsdale, R.L. "An Accelerated Incremental Radiosity Algorithm", Journal of Computer Science and Technology, 2000